

# Energy transfer among distant quantum systems in spatially shaped laser fields: Two H atoms with the internuclear separation of 5.29 nm (100 a.u.)

Guennaddi K. Paramonov, Oliver Kühn

*Institut für Physik, Universität Rostock, 18051 Rostock, Germany*

and André D. Bandrauk

*Laboratoire de Chimie Théorique, Faculté des Sciences,*

*Université de Sherbrooke, Sherbrooke, Québec, Canada J1K 2R1*

The quantum dynamics of two distant H atoms excited by ultrashort and spatially shaped laser pulses is studied by the numerical solution of the non-Born-Oppenheimer time-dependent Schrödinger equation within a three-dimensional (3D) model, including the internuclear distance  $R$  and the two  $z$  coordinates of the electrons,  $z_1$  and  $z_2$ . The two 1D hydrogen atoms, A and B, are assumed to be initially in their ground states with a large (but otherwise arbitrary) internuclear separation of  $R = 100$  a.u. (5.29 nm). Two types of a spatial envelope of a laser field linearly polarized along the  $z$ -axis are considered: (i) a broad Gaussian envelope, such that atom A is excited by the laser field predominantly, and (ii) a narrow envelope, such that practically only atom A is excited by the laser field. With the laser carrier frequency  $\omega = 1.0$  a.u. and the pulse duration  $t_p = 5$  fs, in both cases an efficient energy transfer from atom A to atom B has been found. The ionization of atom B achieved mostly after the end of the laser pulse is close to or even higher than that of atom A. It is shown that with a narrow spatial envelope of the laser field, the underlying mechanisms of the energy transfer from A to B and the ionization of B are the Coulomb attraction of the laser driven electron by the proton of atom B and a short-range Coulomb repulsion of the two electrons when their wave functions significantly overlap in the domain of atom B. In the case of a broad Gaussian spatial envelope of the laser field, the opposite process also occurs, but with smaller probability: the energy is transferred from the weakly excited atom B to atom A, and the ionization of atom A is also induced by the electron-electron repulsion in the domain of atom A due to a strong overlap of the electronic wave functions.

## I. INTRODUCTION

The laser driven dynamics of distant quantum systems can depend in general on the spatial and temporal envelope of the applied laser field. For example, at a gas pressure of 1 atm., the interparticle distance is about 100 a.u. (5.29 nm). If such a system, e.g. composed of H atoms, is excited by a laser field with the carrier frequency  $\omega = 1.0$  a.u., corresponding to the ground-state energy of  $H_2$  at a large internuclear distance  $R$ , the wavelength is  $\lambda = 861$  a.u. (45.56 nm). If the laser field is focused within the diffraction limit onto a spot with the width  $\lambda$ , the Gaussian spatial envelope of the field may result in quite different electric field strengths for H atoms separated by about 100 a.u., especially at the edges of the Gaussian spatial envelope. Although the H atoms are far away from each other, their electron-electron interaction should not be *a priori* neglected, especially upon their excitation by the laser field, because the electronic wave functions extend and vanish, strictly speaking, only at infinity. Therefore, the energy transfer among distant quantum systems, similar to that studied in [1–8], can be anticipated to occur in spatially shaped laser fields as well. For ultrashort laser pulses, containing only few optical cycles, one must also consider the carrier envelope phase (CEP) of the pulse [9].

The long-range energy transfer from an excited atom to its neighbor has been recently studied by Cederbaum *et al.* for molecular clusters [1] and is known as the

interatomic Coulombic decay (ICD). Nowadays, ICD is well established also experimentally for inner-valence excitation of many electron systems [2–6]. In recent work [7], ICD was demonstrated experimentally for a helium dimer. Since helium atoms have no inner-valence electrons, a different type of ICD is operative for this case. It was thus concluded in [7] that since ICD in a helium dimer takes place at interatomic distances up to  $\approx 12$  a.u., no overlap of the electronic wave functions is required for the process.

The present work is addressed to a quantum system composed of two H atoms with the initial internuclear separation of 100 a.u. (5.29 nm) which is excited by spatially shaped laser pulses: spatially broad pulses exciting both H atoms, and spatially narrow pulses exciting only one H atom of the entire H-H system. The relative simplicity of the H-H system under consideration (similar to that used in [10]) makes it possible to treat the long-range electronic motion explicitly together with the nuclear motion such as to reveal the role played by the electron-electron interaction and by the overlap of the electronic wave functions. An example of long-range laser-induced electron transfer (LIET) in the one electron linear  $H^+-H_2^+$  atom-molecule system has been treated previously within the Born-Oppenheimer approximation [11]. Long-range charge and energy transfer can occur also in large molecular systems, as described recently in Ref. [12] and references therein.

The following two types of H-H systems will be distinguished in the present work: (i) a ‘molecular’ H-H

system, representing an elongated configuration of the  $\text{H}_2$  molecule, similar to that studied recently in [13] for long-range entanglement, and (ii) an ‘atomic’ H-H system, representing two distant H atoms. Accordingly, the initial state of a molecular H-H system is assumed to be entangled by spin exchange and represented by the Heitler-London symmetric product of atomic wave functions, while the initial state of an atomic H-H system is not entangled – it is a direct-product state of atomic wave functions. In both cases the excitation of H-H is accomplished by laser pulses with (i) a broad Gaussian spatial envelope, such that both H atoms are excited by the laser field, with atom A being excited predominantly, and (ii) with a narrow spatial envelope, such that only atom A is excited by the laser field.

The paper is organized as follows. The model of the H-H system and techniques used are described in Sec. II. Excitation, energy transfer, and ionization of an unentangled atomic H-H system are presented in Sec. III. Section IV is devoted to the laser-driven dynamics of an entangled molecular H-H system. The results obtained are summarized and discussed in the concluding Section V.

## II. MODEL, EQUATIONS OF MOTION, AND TECHNIQUES

Within the 3D four-body model of H-H excited by the temporally and spatially shaped laser field the total Hamiltonian  $\hat{H}_T$  is divided into two parts,

$$\hat{H}_T(R, z_1, z_2, t) = \hat{H}_S(R, z_1, z_2) + \hat{H}_{\text{SF}}(z_1, z_2, t), \quad (1)$$

where  $\hat{H}_S(R, z_1, z_2)$  represents the H-H system and  $\hat{H}_{\text{SF}}(z_1, z_2, t)$  describes the interaction of the system with the laser field. The applied laser field is assumed to be linearly polarized along the  $z$ -axis, the nuclear and the electronic motion are restricted to the polarization direction of the laser electric field. Accordingly, two  $z$  coordinates of electrons,  $z_1$  and  $z_2$ , measured with respect to the nuclear center of mass, are treated explicitly together with the internuclear distance  $R$ . A similar model has been used previously in [10] for the  $\text{H}_2$  molecule, where each particle, electron or proton, is treated in 1D, i.e.,  $z$  and  $R$ .

The total non-Born-Oppenheimer system Hamiltonian (employing a. u.:  $e = \hbar = m_e = 1$ ) reads

$$\begin{aligned} \hat{H}_S(R, z_1, z_2) = & -\frac{1}{m_p} \frac{\partial^2}{\partial R^2} + V_{\text{pp}}(R) \\ & + \sum_{k=1}^2 \left[ -\frac{1}{2\mu_e} \frac{\partial^2}{\partial z_k^2} + V_{\text{ep}}(z_k, R) \right] + V_{\text{ee}}(z_1, z_2), \end{aligned} \quad (2)$$

where  $m_p$  is the proton mass,  $\mu_e = 2m_p/(2m_p + 1)$  is the reduced electron mass, and non-diagonal mass-

polarization terms are neglected. The Coulomb potentials in Eq. (2) read

$$\begin{aligned} V_{\text{pp}}(R) = \frac{1}{R}, \quad V_{\text{ee}}(z_1, z_2) = \frac{1}{\sqrt{(z_1 - z_2)^2 + \alpha}}, \\ V_{\text{ep}}(z_k, R) = -\frac{1}{\sqrt{(z_k - R/2)^2 + \beta}} - \frac{1}{\sqrt{(z_k + R/2)^2 + \beta}}, \end{aligned} \quad (3)$$

where  $k = 1, 2$ , and the regularization parameters,  $\alpha = 0.1 \times 10^{-3}$  and  $\beta = 1.995$ , have been chosen (similar to previous work [10]) such as to reproduce the ground-state (GS) energy of the H-H system at  $R = 100$  a.u. ( $E_{\text{H-H}}^{\text{GS}} = -1.0$  a.u.).

The interaction of the H-H system with the laser field is treated within the semiclassical electric dipole approximation by the Hamiltonian

$$\hat{H}_{\text{SF}}(z_1, z_2, t) = -\frac{1}{c} \frac{\partial A(t)}{\partial t} (1 + \gamma) \sum_{k=1}^2 F(z_k) z_k, \quad (4)$$

where  $\gamma = (1 + 2m_p)^{-1}$ ,  $A(t)$  is the vector potential,  $c$  is the speed of light, and  $F(z)$  is the spatial-shape function, or envelope, of the laser field. In the general case we set  $F(z_1) = F(z_2)$ , except for some model simulations detailed in Sec. IV.

The vector potential,  $A(t)$ , is chosen in the following form:

$$A(t) = \frac{c}{\omega} \mathcal{E}_0 \sin^2(\pi t/t_p) \cos(\omega t + \phi), \quad (5)$$

where  $\mathcal{E}_0$  is the amplitude,  $t_p$  is the pulse duration at the base,  $\omega$  is the laser carrier frequency, and  $\phi$  is the carrier-envelope phase (CEP). Note that it has been shown previously [9] that the carrier phase of the laser pulse is important only for pulses having less than 15 optical cycles. The definition of the system-field interaction by Eq. (4) via the vector potential, suggested in [13], assures that the electric field  $\mathcal{E}(t) = -\frac{1}{c} \partial A(t)/\partial t$  has a vanishing direct-current component,  $\int_0^{t_p} \mathcal{E}(t) dt = 0$ , and satisfies Maxwell’s equations in the propagation region.

It is suitable to define, on the basis of Eqs. (4) and (5), the local effective-field amplitudes for atoms A and B as follows:

$$\mathcal{E}_0^A = \mathcal{E}_0 F(z_A), \quad \mathcal{E}_0^B = \mathcal{E}_0 F(z_B), \quad (6)$$

where  $z_A = -50$  a.u.,  $z_B = 50$  a.u.. The respective time-dependent electric fields acting on atoms A and B read

$$\begin{aligned} \mathcal{E}^{A,B}(t) = & \mathcal{E}_0^{A,B} [\sin^2(\pi t/t_p) \sin(\omega t + \phi) \\ & - \frac{\pi}{\omega t_p} \sin(2\pi t/t_p) \cos(\omega t + \phi)]. \end{aligned} \quad (7)$$

The first term in Eq. (7) corresponds to a laser pulse with a  $\sin^2$ -type temporal envelope, while the second, the so-called ‘switching’ term, appears due to the finite pulse duration [13, 14].

The 3D time-dependent Schrödinger equation for 1D electrons ( $z_1, z_2$ ) and 1D protons ( $R$ ),

$$i\frac{\partial}{\partial t}\Psi = [\hat{H}_S(R, z_1, z_2) + \hat{H}_{SF}(z_1, z_2, t)]\Psi, \quad (8)$$

has been solved numerically with the propagation technique adapted from [15] for both electron and proton quantum motion. In particular, calculations for the electron motion have been performed by using 200-point non-equidistant grids for the Hermite polynomials and corresponding weights for the numerical integration on the interval  $(-\infty, \infty)$  for the  $z_1$  and  $z_2$  coordinates. For the nuclear coordinate  $R$ , a 256-point equidistant grid has been used on the interval [75 a.u., 125 a.u.]. The time-step of the propagation was  $\Delta t = 0.021$  a.u. (1 a.u.=24 asec).

The wave functions of the initial states have been obtained by numerical propagation of the equation of motion (8) in imaginary time without the laser field ( $\mathcal{E}_0 = 0$ ).

Upon excitation of the H-H system by the laser field, the electronic wave functions of its atomic A and B parts may overlap. In order to study the energy transfer from A to B, the respective ‘atomic’ energies,  $E_A(t)$  and  $E_B(t)$ , are defined on the basis of Eqs. (2) and (3) such that their sum always gives the correct total energy of the entire H-H system. The definitions of ‘atomic’ energies  $E_A(t)$  and  $E_B(t)$  for the H-H systems of atomic and molecular origin are different due to the different symmetry and entanglement of the respective wave functions and will be specified in the following sections.

The ionization probabilities for atoms A and B have been calculated from the time- and space-integrated outgoing fluxes separately for the positive and the negative directions of the  $z_1$  and  $z_2$  axes at  $z_{1,2} = \pm 91$  a.u.. Specifically, we calculated four ionization probabilities:  $I_A(z_1 = -91 \text{ a.u.})$  and  $I_A(z_2 = -91 \text{ a.u.})$  for atom A, and  $I_B(z_1 = 91 \text{ a.u.})$  and  $I_B(z_2 = 91 \text{ a.u.})$  for atom B. At the outer limits of the  $z$ -grids, absorbing boundaries have been provided by imaginary smooth optical potentials adapted from that designed in [16]. Similar optical potentials have been also provided for the  $R$ -axis but, in practice, the wave-packet never approached the outer limits of the  $R$ -grid.

### III. EXCITATION OF H-H FROM AN UNENTANGLED DIRECT-PRODUCT INITIAL STATE

The spatial part of the initial unentangled direct-product ground-state wave function of H-H of an atomic configuration used in the imaginary time propagation is defined with the unsymmetrized Heitler-London electron wave function as follows:

$$\Psi(R, z_1, z_2, t = 0) = \Psi_{1SA}(z_1)\Psi_{1SB}(z_2)\Psi_G(R), \quad (9)$$

where  $\Psi_{1SA}(z_1) = e^{-|z_1 - z_A|}$  at  $z_A = -50$  a.u.,  $\Psi_{1SB}(z_2) = e^{-|z_2 - z_B|}$  at  $z_B = 50$  a.u., and  $\Psi_G(R)$  is a proton Gaussian function centered at  $R = 100$  a.u..

The imaginary-time propagations have been performed with a reduced, ‘non-interacting’ atoms, version of the system Hamiltonian (2) wherein the nuclear  $V_{pp}(R)$  and electronic  $V_{ee}(z_1, z_2)$  terms were omitted and only the Coulombic interaction  $V_{ep}(z_{1(2)}, R)$  of each electron with its nearest proton was taken into account along with the three kinetic-energy terms of Eq. (2). The results obtained gave a direct-product initial state. For the sake of comparison, we have also performed the imaginary-time propagations with the complete system Hamiltonian (2). The results obtained proved to be practically identical to those obtained in the case of two non-interacting H atoms. The energy difference, for example, is less than  $1.8 \times 10^{-5}$  a.u., implying that the Coulombic interaction  $V_{ee}(z_1, z_2)$  of two H atoms in their ground states is negligible at  $R = 100$  a.u..

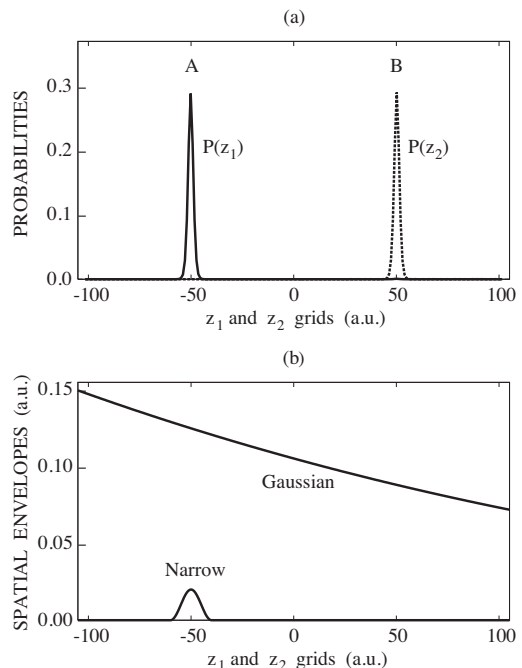


FIG. 1. The initial unentangled direct-product state of the H-H system and the spatial envelopes of the applied laser pulses. (a) - electron probabilities:  $P(z_1)$  is the probability to find electron  $e_1$  initially belonging to atom A at  $z = z_1$  with any values of the other two coordinates,  $R$  and  $z_2$ ; probability  $P(z_2)$  has a similar meaning for electron  $e_2$  initially belonging to atom B; (b) - spatial envelopes of applied laser fields: the broad Gaussian envelope of Eq. (14) and the narrow envelope of Eq. (16).

The initial unentangled direct-product state of the H-H system representing two non-interacting H atoms, A and B, is presented in Fig. 1(a) by the electron probabilities  $P(z_1)$  and  $P(z_2)$ , which are defined as follows:

$$P(z_1) = \int dR \int dz_2 |\Psi(R, z_1, z_2)|^2 \quad (10)$$

for electron  $e_1$  initially belonging to atom A with proton

$p_A$ , and similarly,

$$P(z_2) = \int dR \int dz_1 |\Psi(R, z_1, z_2)|^2, \quad (11)$$

for electron  $e_2$  initially belonging to atom B with proton  $p_B$ . These electron probabilities give the overall probability to find an electron at a specified point of the  $z$ -axis at any position of the other electron and at any internuclear distance.

After calculation of the unentangled initial state of the atomic H-H system, its laser-driven quantum dynamics in real time has been explored with the complete system Hamiltonian of Eq. (2). The spatial envelopes of the applied laser pulses, Gaussian and narrow, defined by Eqs. (14) and Eq. (16) below, are presented in Fig. 1(b) to illustrate the local effective-field strengths acting on atoms A and B.

Two possible choices for the laser carrier frequency are:  $\omega = 0.5$  a.u. (corresponding to the ground-state energy of an H atom), and  $\omega = 1.0$  a.u. (corresponding to the ground-state energy of H-H at large  $R$ ). Our numerical simulations have shown that at  $\omega = 0.5$  a.u., an efficient ionization of A takes place, while the energy transfer from A to B and the ionization of B are not efficient. In contrast, at  $\omega = 1.0$  a.u., the energy transfer from A to B and the ionization of B are efficient. This implies the existence of an optimal laser frequency suitable for the most efficient energy transfer. This issue will be addressed in a forthcoming work; below we present the results obtained at  $\omega = 1.0$  a.u.. With the laser pulse duration  $t_p = 5$  fs, as used throughout this work, the number of optical cycles during the pulse,  $N_c = \omega t_p / 2\pi$ , is about 33. Therefore, the carrier phase of the laser field  $\phi$  is not important [9] and set equal to zero in our simulations below [ $\phi = 0$  in Eqs. (5) and (7)].

In order to study the energy transfer from A to B, the respective ‘atomic’ energies,  $E_A(t)$  and  $E_B(t)$ , have been defined on the basis of Eqs. (2) and (3) as follows:

$$E_A(t) = \left\langle \Psi(t) \left| -\frac{1}{2m_p} \frac{\partial^2}{\partial R^2} + \frac{1}{2} V_{pp}(R) + \frac{1}{2} V_{ee}(z_1, z_2) - \frac{1}{2\mu_e} \frac{\partial^2}{\partial z_1^2} - \sum_{k=1}^2 \frac{1}{\sqrt{(z_k + R/2)^2 + \beta}} \right| \Psi(t) \right\rangle \quad (12)$$

for atom A and similarly,

$$E_B(t) = \left\langle \Psi(t) \left| -\frac{1}{2m_p} \frac{\partial^2}{\partial R^2} + \frac{1}{2} V_{pp}(R) + \frac{1}{2} V_{ee}(z_1, z_2) - \frac{1}{2\mu_e} \frac{\partial^2}{\partial z_2^2} - \sum_{k=1}^2 \frac{1}{\sqrt{(z_k - R/2)^2 + \beta}} \right| \Psi(t) \right\rangle, \quad (13)$$

for atom B. From Eqs. (12) and (13) we see that the kinetic energy of nuclear motion and the potential energies

of the proton-proton and the electron-electron interaction are assumed to be equally shared between atoms A and B. The kinetic energy of electron  $e_1$  and the energy of Coulombic interaction of both electrons,  $e_1$  and  $e_2$ , with proton  $p_A$  are entirely assigned to atom A. Similarly, the kinetic energy of electron  $e_2$  and the energy of Coulombic interaction of both electrons with proton  $p_B$  are entirely assigned to atom B. The sum of ‘atomic’ energies always gives the correct total energy of the entire H-H system. Notice, in particular, that the fact that the kinetic energy of electron  $e_1/e_2$  is entirely assigned to atom A/B corresponds to the initial electron probabilities  $P(z_1)/P(z_2)$  in the unentangled atomic state [Fig. 1(a)]. Indeed, electron  $e_1$  is localized in the vicinity of proton  $p_A$  of atom A and electron  $e_2$  is localized in the vicinity of proton  $p_B$  of atom B. Therefore, if e.g. the laser pulse with a narrow spatial shape [Fig. 1(b)] is used to excite the extended H-H system, only the ‘atomic’ energy  $E_A(t)$  will increase, while  $E_B(t)$  will not be affected.

The left panel of Fig. 2 presents the dynamics of the atomic H-H system excited by the laser pulse with the Gaussian spatial envelope

$$F_G(z) = \exp\{-(z - z_0)/\lambda\}^2, \quad (14)$$

where  $\lambda = 861$  a.u. (45.56 nm) and the laser field is assumed to be focused onto a spot centered at  $z_0$ , where  $z_0 = -1.5\lambda$  [ $z_0 = -1291.5$  a.u. (-68.34 nm)]: cf. Fig. 1(b). The laser pulse parameters are:  $\omega = 1.0$  a.u.,  $t_p = 5$  fs, and  $\mathcal{E}_0 = 1.0$  a.u. ( $\mathcal{E}_0 = 5.14 \times 10^9$  V/cm, intensity  $I_0^A = 3.5 \times 10^{16}$  W/cm<sup>2</sup>). Accordingly, the spatial envelope function  $F(z)$  in the interaction Hamiltonian of Eq. (4) is set equal to  $F_G(z)$  of Eq. (14), and the effective-field amplitudes for atoms A and B defined by Eq. (6) are:  $\mathcal{E}_0^A = 0.125$  a.u. (intensity  $I_0^A = 5.48 \times 10^{14}$  W/cm<sup>2</sup>) and  $\mathcal{E}_0^B = 0.088$  a.u., ( $I_0^B = 2.72 \times 10^{14}$  W/cm<sup>2</sup>), implying a dominant excitation of atom A, which is clearly observed in Fig. 2(a).

From Fig. 2(a) we see that the ‘atomic’ energy  $E_A(t)$  is controlled by the applied laser pulse: it increases in the first half of the pulse and decreases to the end of the pulse. In contrast, the ‘atomic’ energy  $E_B(t)$  does not follow the applied laser pulse: it slowly increases up to the end of the laser pulse and even exceeds  $E_A(t)$  shortly after the end of the pulse. A similar behavior is found for the ‘atomic’ ionizations  $I_A$  and  $I_B$  presented in Fig. 2(b): while the laser-induced ionization  $I_A$  rises fast in the second half of the pulse, the ionization probability  $I_B$  sharply rises after the end of the pulse. Such a behavior will be referred to below as a ‘sequential’ ionization, implying a delayed interaction due to LIET. The time-dependent expectation values  $\langle R(t) \rangle$ ,  $\langle z_1(t) \rangle$  and  $\langle z_2(t) \rangle$  are presented in Fig. 2(c). The time-dependent deviations of the expectation values  $\langle z_1(t) \rangle$  and  $\langle z_2(t) \rangle$ ,

$$\Delta z_1(t) = \langle z_1(t) \rangle - \langle z_1(t=0) \rangle,$$

$$\Delta z_2(t) = \langle z_2(t) \rangle - \langle z_2(t=0) \rangle, \quad (15)$$

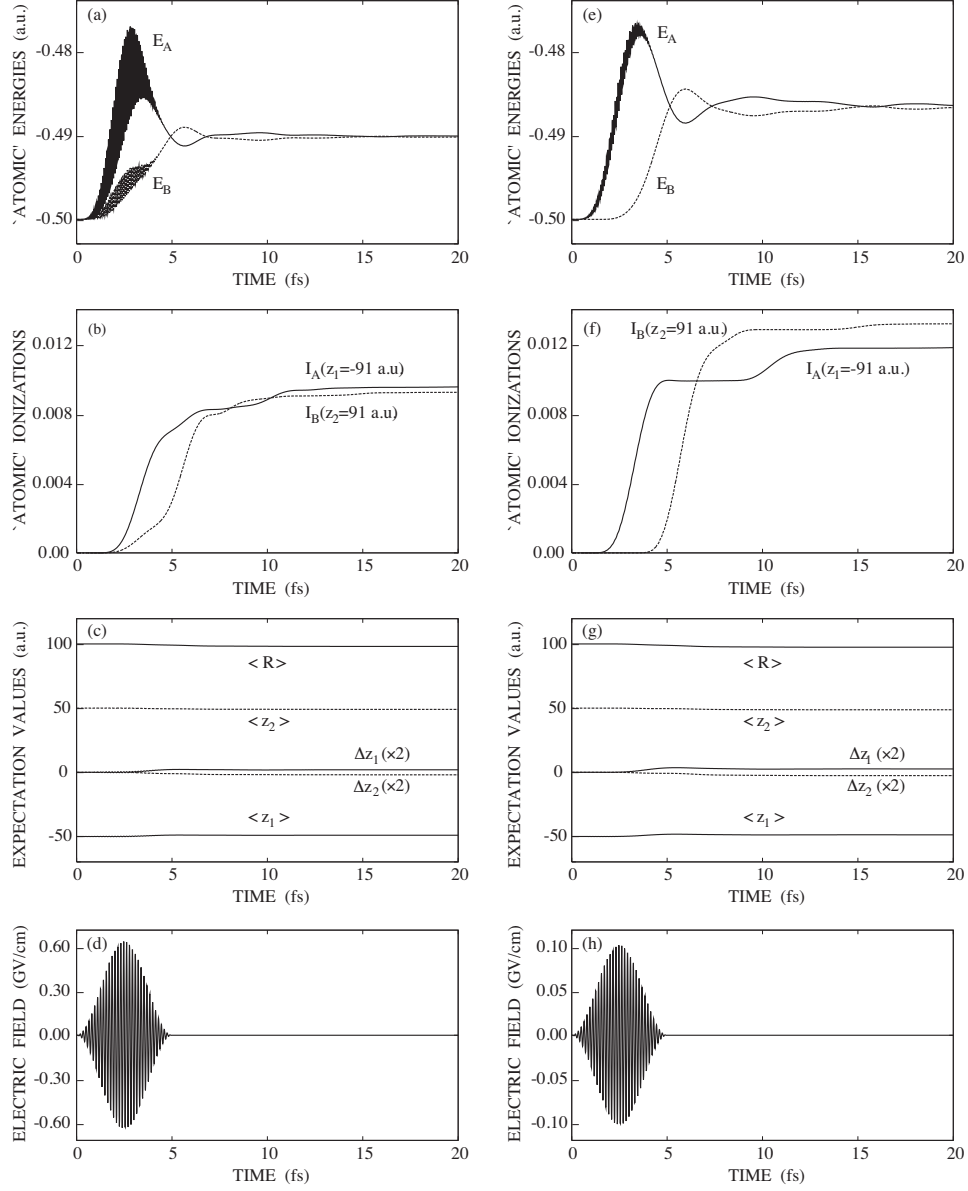


FIG. 2. Quantum dynamics of H-H excited from an unentangled direct-product initial state by spatially shaped laser fields: a Gaussian spatial envelope (a-d) and a narrow spatial envelope (e-f). (a) and (e) - the energy transfer; (b) and (f) - ‘atomic’ ionizations [ionization probabilities  $I_A(z_1 = 91 \text{ a.u.})$  and  $I_B(z_2 = -91 \text{ a.u.})$  are of the order of  $10^{-6}$  and are not shown]; (c) and (g) - expectation values  $\langle R \rangle$ ,  $\langle z_1 \rangle$  and  $\langle z_2 \rangle$  (deviations of the expectation values,  $\Delta z_1$  and  $\Delta z_2$ , defined by Eqs. (15) are scaled up by a factor of two); (d) and (h) - local effective laser fields  $\mathcal{E}^A(t)$  [Eqs. (6) and (7)] acting on atom A.

plotted in Fig. 2(c) are scaled up by a factor of two. We see from Fig. 2(c) that  $\Delta z_1(t) > 0$ , implying attraction of electron  $e_1$  by proton  $p_B$ . In contrast,  $\Delta z_2(t) < 0$ , implying attraction of electron  $e_2$  by proton  $p_A$ . It is also seen from Figs. 2(a), 2(b) and 2(c) that both the energy transfer from A to B and the ‘sequential’ ionization of B in the positive direction of the  $z_2$ -axis correlate with a small decrease of the spatial separation of electrons,  $|\langle z_2 \rangle - \langle z_1 \rangle|$ , such that the electron-electron repulsion (EER) becomes effective.

In order to clarify these findings further, we have performed a similar numerical simulation with a narrow spatial envelope of the laser pulse acting practically only on atom A of the entire H-H system. Specifically, the following  $\sin^2$ -type spatial envelope of the laser pulse was used for  $z = z_1$  and  $z = z_2$ :

$$F_N(z) = \sin^2 \left[ \frac{\pi(z - z_a)}{z_b - z_a} \right], \quad z_a \leq z \leq z_b, \quad (16)$$

where  $z_a = -60 \text{ a.u.}$ ,  $z_b = -40 \text{ a.u.}$ , and  $F_N(z) = 0$  oth-

erwise, as illustrated in Fig. 1(b). Accordingly, the spatial envelope function  $F(z)$  in Eq. (4) is set equal to  $F_N(z)$  of Eq. (16). The amplitude of the pulse,  $\mathcal{E}_0 = 0.02$  a.u. ( $I_0 = 1.4 \times 10^{13}$  W/cm<sup>2</sup>), is chosen such that the ‘atomic’ energy  $E_A(t)$  gained in the field with the narrow spatial envelope [Fig. 2(e)] is close to that gained with the Gaussian spatial envelope [Fig. 2(a)]. Note that, defined by Eq. (7), the effective-field strength  $\mathcal{E}^A(t)$  of the laser pulse with the narrow spatial envelope [Figs. 1(b) and 2(h)] is much smaller than that of the laser pulse with the Gaussian spatial envelope [Figs. 1(b) and 2(d)], but the energy transfer from A to B is by about 30% more efficient [Fig. 2(e)]. Also note that, due to the effective-field amplitude acting on atom B in the current case of the narrow spatial envelope of the pulse is  $\mathcal{E}_0^B = 0$ , the efficient energy transfer to atom B is attributed entirely to the electron-electron repulsion  $V_{ee}(z_1, z_2)$  and electron-proton attraction  $V_{ep}(z_{1(2)}, R)$  in the vicinity of atom B ( $z_{1(2)} = z_B$ ). This also applies to the ionization of atom B in the positive direction of the  $z_2$ -axis [Fig. 2(f)], which is not only by about 30% more efficient than that induced by the laser pulse with the broad Gaussian spatial envelope [Fig. 2(b)], but  $I_B$  is even larger than  $I_A$  at  $t > 7$  fs [Fig. 2(f)], implying that the ‘sequential’ ionization  $I_B$ , induced by EER, is more efficient than the laser-induced ionization  $I_A$ .

Taking into account that in the unentangled direct-product state (9), electrons  $e_1$  and  $e_2$  are well localized on the  $z$ -axis [Fig. 1(a)], one can assume that the time-dependent expectation values  $\langle z_1(t) \rangle$  and  $\langle z_2(t) \rangle$  represent the positions of electrons. A closer look at the data presented in Figs. 2(c) and 2(g) for  $\langle z_1(t) \rangle$  and  $\langle z_2(t) \rangle$  shows that the two electrons of H-H do not approach each other closer than 98 a.u. (5.18 nm). Therefore, at a first glance, the energy transfer from A to B and the ‘sequential’ ionization of B take place, similarly to ICD [1–8], without any noticeable overlap of the respective electronic wave functions. Nevertheless, a closer look at spatial distributions of the electronic wave functions illustrated in Fig. 3 reveals that EER is in fact a short-range process which takes place in the vicinity of atom B at  $z_B = 50$  a.u.. Here, the Coulombic attraction of electron  $e_1$  by proton  $p_B$  effectively localizes electron  $e_1$ . Accordingly, the overlap of the electronic wave functions has a sharp narrow maximum at  $z_B = 50$  a.u. (Fig. 3), which results in a strong EER.

Electron probabilities  $P(z_1)$  and  $P(z_2)$  presented in Fig. 3 correspond to the end of the 5 fs laser pulse with the narrow spatial envelope defined by Eq. (16). This pulse excites practically only electron  $e_1$  in the vicinity of  $z_A = -50$  a.u., therefore the probability distribution  $P(z_1)$  at  $t = 5$  fs is broadened in comparison to the initial one [Fig. 1(a)] in both  $z_1 < z_A$  and  $z_1 > z_A$  directions. The laser-induced extension of  $P(z_1)$  into the domain of  $z_1 < z_A$  gives rise to the ionization  $I_A$  on the negative direction of the  $z_1$ -axis. At  $z_1 \leq -91$  a.u., the wave function is absorbed by the imaginary optical potential. In contrast, at  $z_1 > z_A$ , the laser-driven electron

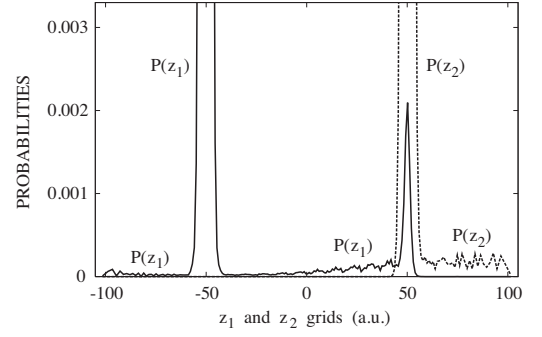


FIG. 3. Electron probabilities  $P(z_1)$  (solid line) and  $P(z_2)$  (dashed line) at the end of the 5 fs laser pulse with a narrow spatial envelope [Eq. (16) and Fig. 1(b)] which excites only electron  $e_1$  (coordinate  $z_1$ ) in the domain of atom A.

$e_1$  reaches the domain  $z_1 > 0$  where it is attracted and accelerated by proton  $p_B$ , localized at  $z_B = 50$  a.u.. Due to the electron-proton Coulombic attraction, the probability  $P(z_1)$  has its local maximum at  $z_1 = z_B$ , corresponding to LIET of Ref. [11]. Simultaneously, when electron  $e_1$  approaches the domain of  $z_B = 50$  a.u., where the initial probability  $P(z_2)$  of electron  $e_2$  has the global maximum [Fig. 1(a)], the electron-electron Coulombic repulsion becomes very strong. Therefore, the probability  $P(z_2)$  is extended into the domain of  $z_2 > z_B$  (Fig. 3), giving rise to the ionization  $I_B$  in the positive direction of the  $z_2$ -axis. Finally, the wave function is absorbed by the imaginary optical potential at  $z_2 \geq 91$  a.u.. Note that in the current case of a narrow spatial envelope of the laser field [Fig. 1(b)] one can clearly distinguish between the laser-induced ionization on the negative direction of the  $z_1$ -axis, represented in Fig. 2(f) by  $I_A(z_1 = -91$  a.u.), and the ‘sequential’ EER-induced ionization on the positive direction of the  $z_2$ -axis, represented in Fig. 2(f) by  $I_B(z_2 = 91$  a.u.). Also note that the ionization probabilities  $I_A(z_1 = 91$  a.u.) and  $I_B(z_2 = -91$  a.u.) are less than  $10^{-6}$  at  $t = 5$  fs.

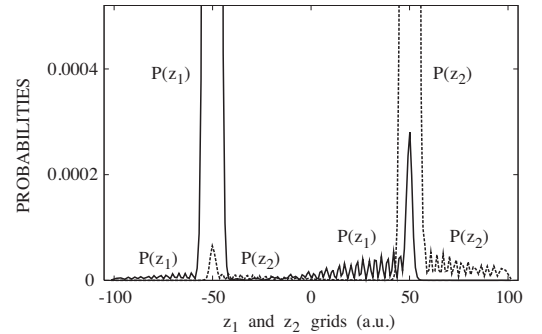


FIG. 4. Electron probabilities  $P(z_1)$  (solid line) and  $P(z_2)$  (dashed line) at 2.5 fs after the end of the 5 fs laser pulse with a Gaussian spatial envelope which excites both electrons, with the excitation of electron  $e_1$  (coordinate  $z_1$ ) being dominant in comparison to that of electron  $e_2$  (coordinate  $z_2$ ).

In the case of the broad Gaussian spatial envelope of the laser pulse centered at  $z_0 = -1291.5$  a.u. ( $-68.34$  nm), both electrons,  $e_1$  and  $e_2$ , are excited by the laser field and therefore ionization in both positive and negative directions of the  $z$ -axis is induced by both the laser field and subsequently by EER. The electron probabilities  $P(z_1)$  (solid line) and  $P(z_2)$  (dashed line) for the Gaussian spatial envelope of the 5 fs laser pulse are plotted in Fig. 4 at  $t = 7.5$  fs, when both ionization probabilities plotted in Fig. 2(b) approach their maximum values. Although both electrons are excited by the laser field, the excitation of electron  $e_1$  in the domain of atom A is about 1.4 times stronger than the excitation of electron  $e_2$  in the domain of atom B. Accordingly, the local maximum of  $P(z_1)$  at  $z_B = 50$  a.u. (Fig. 4) is almost 4 times higher than the local maximum of  $P(z_2)$  at  $z_A = -50$  a.u. and therefore the EER-induced ionization in the positive direction of the  $z_2$ -axis is stronger than the EER-induced ionization in the negative direction of the  $z_1$ -axis. In contrast, the laser-induced ionization in the negative direction of the  $z_1$ -axis is stronger than that in the positive direction of the  $z_2$ -axis. Indeed, it is seen from Fig. 2(b) that at the end of the 5 fs laser pulse, the ionization probability  $I_B$  is more than twice smaller than  $I_A$ , while  $I_B \approx I_A$  at  $t > 10$  fs.

It is seen from Fig. 4 that both local maxima,  $P(z_1)$  at  $z_1 = -50$  a.u. and  $P(z_2)$  at  $z_2 = 50$  a.u., are significantly smaller than the local maximum of  $P(z_1)$  at  $z_1 = -50$  a.u. produced by the laser pulse with a narrow spatial envelope (see Fig. 3). Therefore the EER-induced ionization in the case of the broad Gaussian spatial envelope of the laser pulse [Fig. 2(b)] is smaller than that in the case of the narrow spatial envelope of the pulse [Fig. 2(f)].

It can be concluded from Fig. 4 that in the general case, when both distant atoms are excited by the laser field, energy is transferred from A to B and from B to A, and EER-induced ionization occurs in both A and B parts of H-H along with the laser-induced ionization. If, for example, the laser pulse has a wide Gaussian spatial envelope and/or is centered at  $z = 0$ , the mutual energy transfers and the EER-induced ionization probabilities are substantial for both distant atoms A and B even at a large internuclear separation.

Finally we note that the appearance of sharp local maxima of  $P(z_1)$  at  $z_1 = 50$  a.u. and of  $P(z_2)$  at  $z_2 = -50$  a.u. (see Figs. 3 and 4) confirm spreading, delocalization, and non-factorization of the initially factorized and well localized on the  $z$ -axis wave function of H-H [Fig. 1(a)] and can therefore [17] be treated as the emergence of long-range entanglement, or quantum non-local connection, at  $R = 100$  a.u.. Recently this long-range entanglement attracted considerable interest both in theory and experiment [13, 18–21].

#### IV. EXCITATION OF H-H FROM AN ENTANGLED INITIAL STATE

The H-H molecular system represents an elongated configuration of the  $H_2$  molecule. Therefore, its initial electronic ground state is entangled via exchange [7, 10, 20]. The spatial part of the initial entangled ground-state wave function of H-H for a singlet electronic state is given by

$$\Psi(R, z_1, z_2, t = 0) = [\Psi_{1SA}(z_1)\Psi_{1SB}(z_2) + \Psi_{1SB}(z_1)\Psi_{1SA}(z_2)]\Psi_G(R), \quad (17)$$

where  $\Psi_{1SA,B}(z_{1,2})$  are defined by Eq. (9) and  $\Psi_G(R)$  is a proton Gaussian function centered at  $R = 100$  a.u.. Imaginary time propagations have been performed with the complete system Hamiltonian (2). In the entangled initial state of the H-H system, electron probabilities  $P(z_1)$  and  $P(z_2)$  are identical to each other.

For the simulations with this entangled initial state (17), the ‘atomic’ energies  $E_A(t)$  and  $E_B(t)$  are defined on the basis of Eqs. (2) and (3) as follows:

$$E_A(t) = \left\langle \Psi(t) \left| -\frac{1}{2m_p} \frac{\partial^2}{\partial R^2} - \frac{1}{2} \sum_{k=1}^2 \frac{1}{2\mu_e} \frac{\partial^2}{\partial z_k^2} + \frac{1}{2} V_{pp}(R) + \frac{1}{2} V_{ee}(z_1, z_2) - \sum_{k=1}^2 \frac{1}{\sqrt{(z_k + R/2)^2 + \beta}} \right| \Psi(t) \right\rangle \quad (18)$$

for atom A, and

$$E_B(t) = \left\langle \Psi(t) \left| -\frac{1}{2m_p} \frac{\partial^2}{\partial R^2} - \frac{1}{2} \sum_{k=1}^2 \frac{1}{2\mu_e} \frac{\partial^2}{\partial z_k^2} + \frac{1}{2} V_{pp}(R) + \frac{1}{2} V_{ee}(z_1, z_2) - \sum_{k=1}^2 \frac{1}{\sqrt{(z_k - R/2)^2 + \beta}} \right| \Psi(t) \right\rangle \quad (19)$$

for atom B. From Eqs. (18) and (19) we see that the kinetic energies of nuclear and electronic motion as well as the potential energies of the proton-proton and the electron-electron Coulombic interaction are assumed to be equally shared between atoms A and B. The energy of Coulombic interaction of both electrons with proton  $p_A$  is assigned to atom A, while the energy of Coulombic interaction of both electrons with proton  $p_B$  is assigned to atom B. The sum of these ‘atomic’ energies always gives the correct total energy of the entire H-H system. The choice of the electron kinetic energies in Eqs. (18) and (19) corresponds to the initial electron probabilities  $P(z_1)$  and  $P(z_2)$  in the entangled molecular state. Both electrons  $e_1$  and  $e_2$  are localized with the 50% probability in the vicinity of proton  $p_A$  of atom A and if the extended H-H system is excited e.g. by the narrowly shaped laser



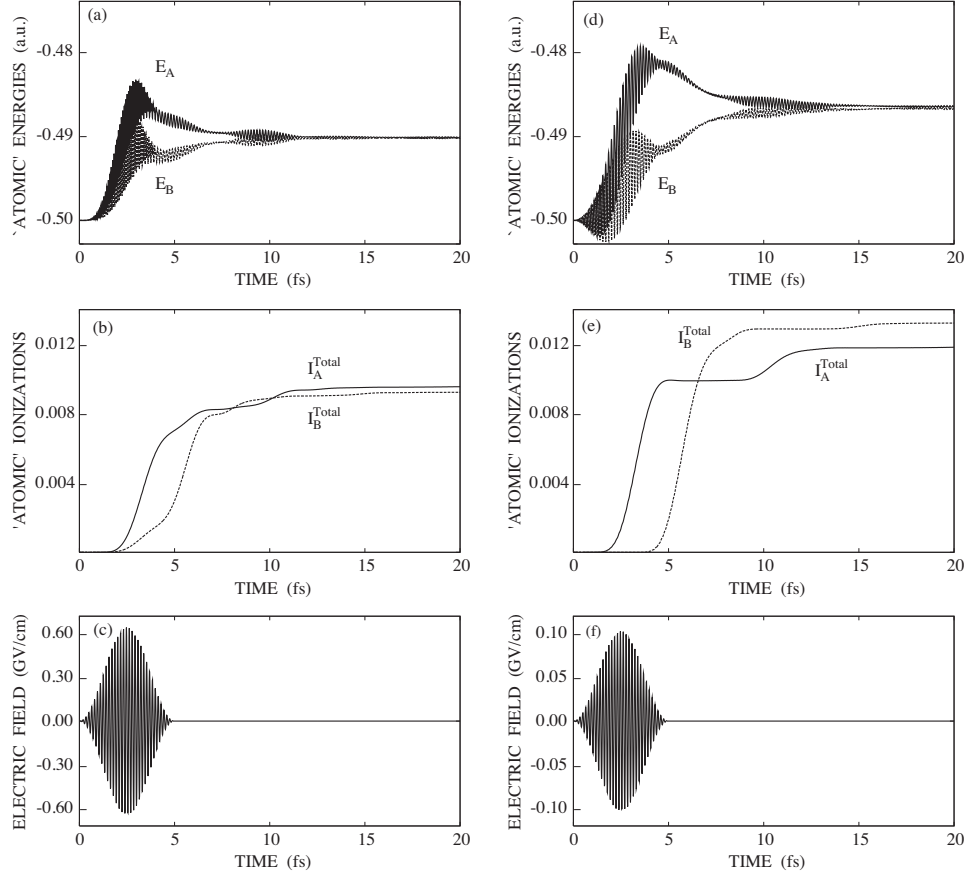


FIG. 5. Quantum dynamics of H-H excited from the entangled initial state (17) by spatially shaped laser fields [Fig. 1(b)]: a broad Gaussian spatial envelope (left panel) and a narrow spatial envelope (right panel). (a) and (d) - the energy transfer; (b) and (e) - ‘atomic’ ionizations; [the total ionization probabilities  $I_A^{\text{Total}}$  and  $I_B^{\text{Total}}$  are defined by Eq. (20)]; (c) and (f) - local effective laser fields  $\mathcal{E}^A(t)$  [Eqs. (6) and (7)] acting on atom A.

pulse of Fig. 1(b), both electrons give rise to the ‘atomic’ energy  $E_A(t)$ , each with 50% probability.

The quantum dynamics of H-H excited from the entangled initial state (17) by spatially shaped laser pulses is presented in Fig. 5. The left panel corresponds to the broad Gaussian spatial envelope centered at  $z_0 = -1291.5$  a.u. (-68.34 nm) and the right panel corresponds to the narrow spatial envelope centered at  $z_A = -50$  a.u. (-2.65 nm), see Fig. 1(b). For the sake of comparison, the laser fields used are the same as in the previous case of the unentangled direct-product initial state [see Figs. 1(b) and 2]. Specifically, the Gaussian spatial envelope is defined by Eq. (14), the narrow spatial envelope is defined by Eq. (16), the carrier frequency of the laser pulse with the  $\sin^2$ -type temporal envelope of Eq. (7) is  $\omega = 1.0$  a.u., and the pulse duration at the base is  $t_p = 5$  fs.

From the comparison of the quantum dynamics of the unentangled state [Figs. 2(a) and 2(e)] to that of the entangled state [Figs. 5(a) and 5(d)] the following observations are made.

(i) The overall energy  $\Delta E_B$  transferred on a long

timescale of  $t = 20$  fs from atom A to atom B in the entangled state is very similar to that transferred from A to B in the unentangled direct-product state:  $\Delta E_B \approx 0.01$  a.u. for the broad Gaussian spatial envelope, and  $\Delta E_B \approx 0.013$  a.u. for the narrow spatial envelope.

(ii) The maximum ‘atomic’ energy  $E_A(t)$  gained during the laser pulse by atom A in the entangled state is smaller than that gained in the unentangled direct-product state. In contrast, the maximum ‘atomic’ energy  $E_B(t)$  gained during the pulse by atom B in the entangled state is substantially larger than that gained in the unentangled direct-product state.

(iii) Moreover, in the case of the entangled initial state, the ‘atomic’ energy  $E_B(t)$  is controlled by the laser pulse similarly to  $E_A(t)$ , even when only atom A is excited by the laser pulse with a narrow spatial envelope: the energy  $E_B(t)$  increases in the first half of the laser pulse and decreases at the end of the pulse, in contrast to the case of the unentangled direct-product initial state. This observation implies that the changes made by the applied



laser field to the entangled wave function in the domain of atom A at  $z_{1,2} \approx -50$  a.u. result in simultaneous changes in atom B at  $z_{1,2} \approx 50$  a.u. due to the symmetry of the wave function by exchange. Such an entangled behaviour is very important for a long-range quantum communication among distant quantum systems [19].

(iv) After the end of the laser pulse, the ‘atomic’ energies  $E_A(t)$  and  $E_B(t)$  demonstrate out-of-phase oscillations: slow oscillations in the case of the unentangled direct-product initial state [Figs. 2(a) and 2(e)] and slow oscillations modulated with very fast ones in the case of the entangled initial state [Figs. 5(a) and 5(d)]. The amplitudes of both slow and fast oscillations of  $E_A(t)$  and  $E_B(t)$  decrease with time, which may indicate the formation of a quasi-stable configuration of the excited H-H system.

It is instructive, before proceeding, to consider the laser-driven dynamics of the entangled H-H system in the initial stage of its excitation by the laser pulse with a narrow spatial envelope (16) which excites electrons  $e_1$  and  $e_2$  only in the domain of atom A. In Fig. 6, the laser-driven dynamics of entangled H-H is presented on the timescale of 1 fs. Time-dependent ‘atomic’ energies,  $E_A(t)$  and  $E_B(t)$ , and expectation values of electronic coordinates,  $\langle z_1(t) \rangle$  and  $\langle z_2(t) \rangle$ , are shown in Figs. 6(a) and 6(b) respectively. The time-dependent laser field is shown in Fig. 6(c).

It is seen from Fig. 6(a) that the ‘atomic’ energies  $E_A(t)$  and  $E_B(t)$  oscillate out-of-phase with respect to each other, with  $E_A(t)$  being in-phase and  $E_B(t)$  being out-of-phase with the applied laser field [Fig. 6(c)].

As seen from Figs. 6(b) and 6(c) the electrons also follow the applied laser field. Note that expectation values  $\langle z_1(t) \rangle$  and  $\langle z_2(t) \rangle$  in the entangled H-H system are identical and not distinguishable in Fig. 6(b). A perfect electron-field following at the laser carrier frequency being as high as 1 a.u. is very interesting. Previously, the electron-field following on the level of expectation values of electronic coordinates have been explored only in the infrared [15] and near-infrared [22] domains of the laser carrier frequency. The electron-field following at high laser frequencies is reminiscent of the well-known recollision model of Corkum [23]. However, an important feature of Fig. 6(b) is that electrons follow the applied laser field in-phase, while according to the theoretical model used in [23] and numerical results of [15] electrons follow the field out-of-phase:  $\langle z(t) \rangle$  decreases when electric-field strength  $\mathcal{E}(t)$  increases. A detailed study of the electron dynamics showed that, probably due to their finite albeit very small mass, the electron do not react to the first half-cycle of the applied field at  $\omega = 1$  a.u. and follows the field in-phase at  $t > 0.15$  fs. On the other hand, the out-of-phase electron-field following take place at  $\omega < 0.1$  a.u.. Similar results have been obtained for the unentangled H-H system excited by the laser pulse with a narrow spatial envelope: the electron  $e_1$  of atom A follows the applied field in-phase at  $\omega = 1$  a.u. and out-of-phase at  $\omega < 0.1$  a.u.. These results can be explained

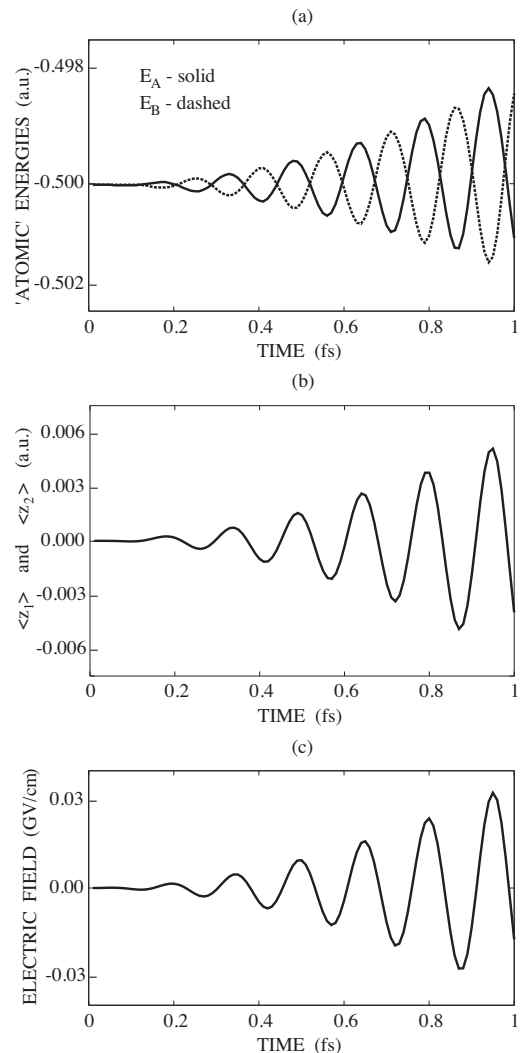


FIG. 6. The initial (1 fs) stage of excitation of H-H from the entangled initial state [Eq. (17)] by the laser pulse with a narrow spatial envelope [Eq. (16)] acting on atom A. (a) - time-dependent ‘atomic’ energies  $E_A(t)$  (solid line) and  $E_B(t)$  (dashed line); (b) - electron-field in-phase following; (c) - the laser field acting on atom A.

as follows. At  $\omega < 0.1$  a.u., the electron is in the ground state, the polarizability is negative and, therefore, the electron follows the applied laser field out-of-phase. In contrast, at  $\omega = 1$  a.u., the electron is well above the excited state, the polarizability changes the sign, and electron follows the field in-phase. Similar behaviour has been observed in a recent work [24] for molecular ion  $\text{H}_2^+$  excited at wavelength  $\lambda = 800$  nm ( $\omega = 0.057$  a.u.). At fixed  $R = 2$  a.u., the electron is in the ground state and follows the field out-of-phase, whereas at  $R = 7$  a.u., the laser carrier frequency  $\omega = 0.057$  a.u. is larger than the energy difference  $E_{1s\sigma_u} - E_{1s\sigma_g}$ , and the electron follows the field in-phase.

Coming back to the laser-driven dynamics of the entan-

gled H-H system on the long timescale of 20 fs (Fig. 5), we note that ionization of atom B starts only in the second half of the laser pulse [see Figs. 5(b) and 5(e)]. Due to the symmetry of the entangled wave function, the ionization probabilities of electrons  $e_1$  and  $e_2$  are identical to each other both for the positive and the negative directions of the  $z$ -axes:  $I_A(z_1 = -91 \text{ a.u.}) = I_A(z_2 = -91 \text{ a.u.})$  and  $I_B(z_1 = 91 \text{ a.u.}) = I_B(z_2 = 91 \text{ a.u.})$ . Therefore, in Figs. 5(b) and 5(e) the total ionization probabilities,

$$I_A^{\text{Total}} = I_A(z_1 = -91 \text{ a.u.}) + I_A(z_2 = -91 \text{ a.u.}),$$

$$I_B^{\text{Total}} = I_B(z_1 = 91 \text{ a.u.}) + I_B(z_2 = 91 \text{ a.u.}), \quad (20)$$

are plotted. From the comparison of Figs. 2(b) and 2(f) to Figs. 5(b) and 5(e) one can easily see that the total time-dependent ionization probabilities  $I_A^{\text{Total}}$  and  $I_B^{\text{Total}}$  used in the case of the entangled initial state are almost equal (but not identical) to the time-dependent ionization probabilities  $I_A(z_1 = -91 \text{ a.u.})$  and  $I_B(z_2 = 91 \text{ a.u.})$  used in the case of the unentangled direct-product initial state. One can conclude therefore that the entanglement of the initial state of H-H, including its exchange symmetry, does not change its ionization probability in comparison to the non-symmetric unentangled direct-product initial state.

The other consequence of the exchange symmetry of the entangled wave function is a very small spatial separation of electrons all over the  $z$ -grid. The time-dependent expectation values  $\langle z_1(t) \rangle$  and  $\langle z_2(t) \rangle$  are almost identical, both being close to 0 on the timescale of 20 fs. If the perfect symmetry of the wave functions is even slightly changed due to the excitation of H-H by the laser field, the very small spatial separation of the electrons leads to their strong Coulombic repulsion all over the  $z$ -grid. This suggests the reason for the fast out-of-phase oscillations of ‘atomic’ energies  $E_A(t)$  and  $E_B(t)$  after the end of the laser pulse [see observation (iv) above and Figs. 5(a) and 5(d)]. The fast out-of-phase oscillations of the ‘atomic’ energies occur in the case of the entangled initial state and do not occur in the case of the unentangled direct-product initial state [Figs. 2(a) and 2(e)]. In the case of the direct-product initial state, the minimum difference between  $\langle z_1(t) \rangle$  and  $\langle z_2(t) \rangle$  is about 98 a.u. (5.18 nm) [see Figs. 2(c) and 2(g)], therefore EER is very weak all over the  $z$ -grid, except for the special cases of very sharp overlaps of the electronic wave functions in the vicinity of protons  $p_A$  and  $p_B$  (see Figs. 3 and 4).

A very strong EER taking place in the case of the entangled initial state should also result in a very efficient EER-induced ‘sequential’ ionization, similar to that described in Sec. III for the unentangled direct-product initial state of H-H. On the other hand, it was shown above that the entanglement of the initial state of H-H does not change its ionization probability in comparison to the direct-product initial state. Therefore, a closer look at the process of EER-induced ionization in the case of

the entangled initial state is required. To this end, we performed several model simulations with the entangled initial state excited in the domain of atom A by the laser pulses with narrow spatial envelopes defined by Eq. (16) for various model assumptions of the system-field interaction to be specified below. The results obtained are presented in Figs. 7 and 8.

Electron probabilities  $P(z_1)$  and  $P(z_2)$  presented in Figs. 7(a) and 7(b) correspond to the end of the 5 fs laser pulse with a narrow spatial envelope [Fig. 1(b)] which excites both electrons  $e_1$  and  $e_2$  in the vicinity of  $z_A = -50 \text{ a.u.}$  (atom A) and does not affect electrons  $e_1$  and  $e_2$  in the vicinity of  $z_B = 50 \text{ a.u.}$  (atom B). Apparently, electron probabilities  $P(z_1)$  and  $P(z_2)$ , presented in Figs. 7(a) and 7(b) at  $t = 5 \text{ fs}$ , are extended in comparison to their initial ones in both  $z_{1,2} < z_A$  and  $z_{1,2} > z_A$  directions. The laser-induced extension of  $P(z_1)$  and  $P(z_2)$  into domains  $z_{1,2} < z_A$  gives rise to the ionization  $I_A$  in the negative directions of the  $z_{1,2}$ -axes. At  $z_{1,2} \leq -91 \text{ a.u.}$ , the wave function is absorbed by the imaginary optical potentials. In contrast, at  $z_{1,2} > z_A$ , the laser-driven electrons  $e_1$  and  $e_2$  reach the domains  $z_{1,2} > 0$  where they are attracted and accelerated by proton  $p_B$ , localized at  $z_B = 50 \text{ a.u.}$ , more and more efficiently. Due to the electron-proton Coulomb attraction, electron probabilities  $P(z_1)$  and  $P(z_2)$  increase in the vicinity of  $z_{1,2} = z_B$  and thus destroy the initially perfect symmetry of the entangled wave function, as clearly seen from Figs. 7(a) and 7(b). The extension of electron probabilities  $P(z_1)$  and  $P(z_2)$  into the domains of  $z_{1,2} > z_B$  gives rise to the EER-induced ‘sequential’ ionization  $I_B$  in the positive directions of the  $z_{1,2}$ -axes. The only problem to be clarified now is EER in the domain of atom B, because at a first glance one could conclude from Figs. 7(a) and 7(b) that the electrons coming from atom A to atom B occupy the domains of  $z_{1,2} > z_B$ . In order to clarify this issue, we performed two model simulations with a 5 fs laser pulse having narrow spatial envelope, assuming that only one of the two electrons is excited by the laser field in the domain of atom A. The results obtained are presented in Figs. 7(c) and 7(d).

First we assume that only electron  $e_1$  is excited by the laser field in the domain of atom A. To this end, we chose the spatial envelope function  $F(z)$  in the interaction Hamiltonian of Eq. (4) as follows:  $F(z_1) = F_N(z_1)$  and  $F(z_2) = 0$ , where the narrow spatial envelope  $F_N(z)$  is given by Eq. (16) and illustrated in Fig. 1(b). The respective electron probabilities  $P(z_1)$  and  $P(z_2)$  at the end of the pulse ( $t = 5 \text{ fs}$ ) are shown in Fig. 7(c). Secondly, we assume that only electron  $e_2$  is excited by the laser field in the domain of atom A. Accordingly, the spatial envelope function  $F(z)$  in the interaction Hamiltonian of Eq. (4) is chosen as follows:  $F(z_1) = 0$ , and  $F(z_2) = F_N(z_2)$ . The respective electron probabilities  $P(z_1)$  and  $P(z_2)$  at the end of the pulse ( $t = 5 \text{ fs}$ ) are shown in Fig. 7(d).

It is seen from the results presented in Figs. 7(c) and 7(d) that the EER-induced ionization of atom B with

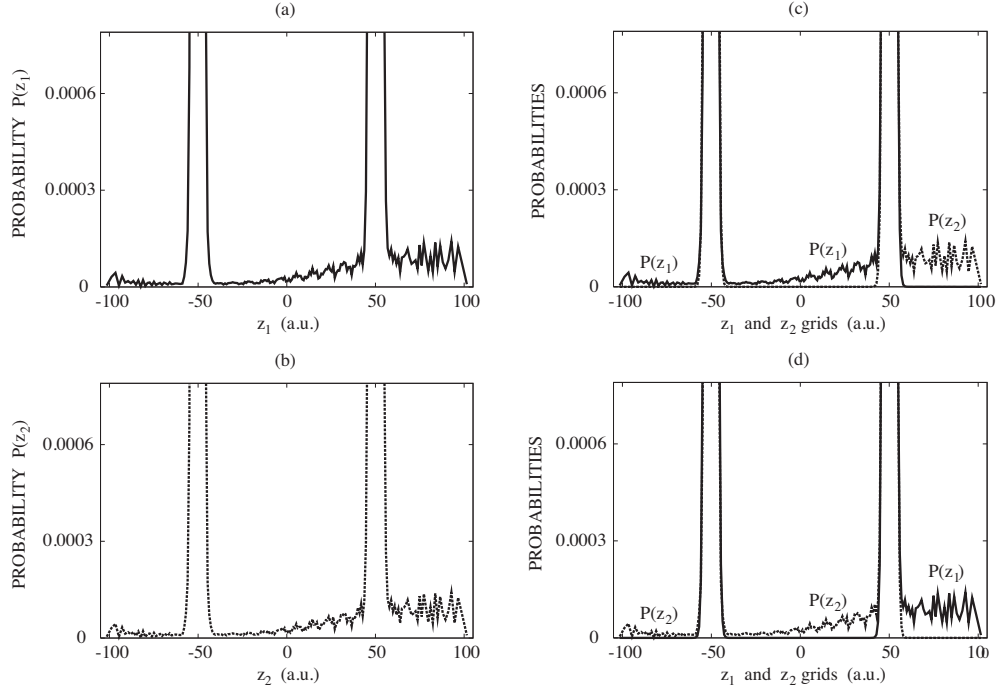


FIG. 7. Excitation of H-H by the laser pulses with the narrow spatial envelopes from the entangled initial state: electron probabilities  $P(z_1)$  (solid lines) and  $P(z_2)$  (dashed lines) at the end of the 5 fs laser pulses. (a) and (b) - both electrons  $e_1$  and  $e_2$  are excited by the laser pulse in the domain of atom A; (c) - only electron  $e_1$  is excited by the laser pulse in the domain of atom A; (d) - only electron  $e_2$  is excited by the laser pulse in the domain of atom A.

the entangled initial state proceeds similar to that with the unentangled direct-product initial state described in Sec. III above. Specifically, [see Fig. 7(c)] the laser-driven electron  $e_1$  (coordinate  $z_1$ ) comes from atom A to atom B and pushes electron  $e_2$  (coordinate  $z_2$ ) out into the domain  $z_2 > z_B$ , where the EER-induced ionization of electron  $e_2$  takes place in the positive direction of the  $z_2$ -axis. At the same time, electron  $e_1$  which arrived at atom B does not affect the probability  $P(z_1)$  at  $z_1 > 50$  a.u.. Similarly, [Fig. 7(d)], the laser-driven electron  $e_2$  (coordinate  $z_2$ ), coming from atom A to atom B, pushes electron  $e_1$  (coordinate  $z_1$ ) into the domain  $z_1 > z_B$ , where the EER-induced ionization of electron  $e_1$  takes place in the positive direction of the  $z_1$ -axis. Electron  $e_2$  does not affect the probability  $P(z_2)$  at  $z_2 > 50$  a.u.. In a realistic case, when both electrons are excited by the laser field [Figs. 7(a) and 7(b)], both processes take place simultaneously.

To identify local maxima of electronic wave functions, we next define the probability differences for electrons,  $\Delta P(z_1, t)$  and  $\Delta P(z_2, t)$ , with respect to the initial electronic probabilities as follows:

$$\Delta P(z_1, t) = P(z_1, t) - P(z_1, t = 0),$$

$$\Delta P(z_2, t) = P(z_2, t) - P(z_2, t = 0). \quad (21)$$

The probability differences  $\Delta P(z_1)$  and  $\Delta P(z_2)$  plotted in Fig. 8 are calculated at the end of the 5 fs laser pulse

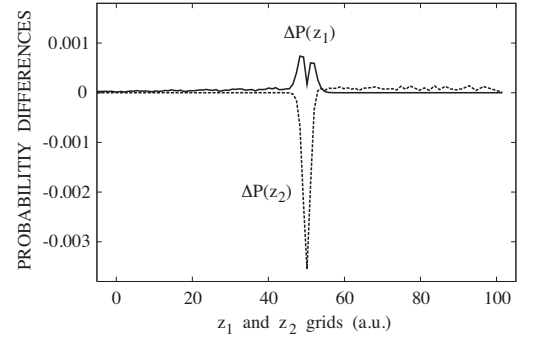


FIG. 8. Excitation of H-H from the entangled initial state by the laser pulse with a narrow spatial envelope which affects only electron  $e_1$  in the domain of atom A: probability differences  $\Delta P(z_1)$  (solid line) and  $\Delta P(z_2)$  (dashed line) in the domain of atom B at the end of the 5 fs laser pulse. The changes of the electron probabilities  $P(z_1)$  and  $P(z_2)$  are measured with respect to their initial values at  $t = 0$  [see Eq. (21)].

with a narrow spatial envelope which excites in the domain of atom A only electron  $e_1$  and does not affect electron  $e_2$ . It can be concluded from Figs. 7(c) and 8 that the laser-driven electron  $e_1$ , coming to the domain  $z_1 > 0$ , is attracted and accelerated therein by proton  $p_B$  and forms at  $t = 5$  fs a local double-peak maximum at  $z_B = 50$  a.u., where electron  $e_2$  already has its global

maximum. Due to a very strong Coulombic repulsion of the two electrons in the vicinity of  $z_B = 50$  a.u., a sharp hole appears in the global maximum of  $P(z_2)$  at the expense of the increasing electron probability  $P(z_2)$  in the domain of  $z_2 > z_B$ , thus giving rise to the EER-induced ionization of electron  $e_2$  in the positive direction of the  $z_2$ -axis. A similar process takes place when only electron  $e_2$  is excited by the laser pulse with a narrow spatial envelope, giving rise to the EER-induced ionization of electron  $e_1$  in the positive direction of the  $z_1$ -axis. In a realistic case, when both electrons are excited by the laser field in the domain of atom A, both described above processes take place simultaneously.

We conclude from the results presented in Figs. 7 and 8 that the physical reasons of the energy transfer from atom A to atom B and the ‘sequential’ ionization of atom B in the case of the entangled initial state and a laser pulse with a narrow spatial envelope, which excites only electrons of atom A, are similar to those underlying the case of the direct-product initial state: the Coulombic attraction of the laser-driven electrons by proton  $p_B$ , and the short-range Coulombic repulsion of the two electrons in the vicinity of proton  $p_B$ , where their wave functions strongly overlap.

## V. CONCLUSION

In the present work we have studied numerically the non-Born-Oppenheimer quantum dynamics of two distant H atoms (being referred to as atoms A and B) with an arbitrary large initial internuclear separation of  $R = 100$  a.u. (5.29 nm), which have been excited by spatially shaped laser pulses. We have found an efficient energy transfer from one H atom to the other and a ‘sequential’ ionization of the latter, induced by a short-range EER. The short-range EER, taking place e.g. in the vicinity of proton  $p_B$  of atom B, occurs due to the preceding long-range LIET from atom A to atom B enhanced by the Coulombic attraction and acceleration of the laser-driven electrons by proton  $p_B$ .

Both unentangled direct-product atomic states and entangled molecular states have been used as the initial states of the H-H system in our numerical simulations. The first case, unentangled atomic states, is more likely to arise in an experiment: at a gas pressure of 1 atm., for example, the interatomic distance is about 100 a.u.. The second case, entangled molecular states, requires an additional step: dissociation of the  $H_2$  molecule, or generation of entanglement between two individual atoms. The field strengths of the spatially shaped laser pulses were chosen such as not to induce a strong ionization and the respective decrease of the overall norm of the wave packet of H-H. In stronger fields and with longer pulses both the energy transfer and the ‘sequential’ ionization can be more efficient than those presented above. The parameters of the laser pulses used in the present work (in particular the pulse duration,  $t_p = 5$  fs, and es-

pecially the laser carrier frequency,  $\omega = 1.0$  a.u.) are not yet optimal, and more efforts will be required in order to find optimal spatially shaped laser fields suitable for the most efficient energy transfer and ‘sequential’ ionization.

We have shown that in the case of a narrow spatial envelope of the applied laser field, when only electrons initially belonging to atom A are excited by the laser field, the physical mechanisms of the energy transfer from atom A to atom B and the ‘sequential’ ionization of atom B are as follows: (i) the Coulombic attraction of the laser-driven electrons by proton  $p_B$  of atom B, resulting in the formation of narrow local maxima of the electronic wave functions in the vicinity of proton  $p_B$ , and (ii) the short-range Coulomb repulsion of the two electrons in the vicinity of proton  $p_B$ , where their wave functions strongly overlap. In a more general case of a wide spatial envelope of the laser field, for example a broad Gaussian, when both A and B atoms are excited by the field simultaneously, the same processes occur in the opposite direction as well: the energy is also transferred from atom B to atom A and the EER-induced ‘sequential’ ionization also occurs in atom A.

Furthermore, we have shown that long-range entanglement of the initially unentangled direct-product state is established by the interaction with a spatially shaped laser pulse. Long-range entanglement attracts considerable interest these days. For example, entanglement transfer from dissociated molecules to photons has been explored in [18], where the concept of transferring the quantum state of two dissociated fragments sharing internal-translational entanglement to that of two photons and vice versa has been put forward. A special kind of an entangled state of one electron and two protons in a  $H_2^+$  molecule adiabatically stretched to  $R = 20 - 100$  a.u. (1.06-5.29 nm) has been studied recently in [13]. A quantum-gate mechanism based on electron spins in coupled semiconductor quantum dots, separated by 40 nm, has been considered in [19] as an important application of long-range entanglement. Such gates provide a source of spin entanglement and can be used for quantum computers. Experimental generation of entanglement between two individual  $^{87}\text{Rb}$  atoms held in two optical tweezers, separated by 4  $\mu\text{m}$ , has been reported in [20]. Finally we mention that quantum entanglement among extended biomolecules has been explored in [21] (see also references therein). The results obtained in [21] demonstrate that there exists robust quantum entanglement among chlorophyll molecules under physiological conditions for the case of a single elementary excitation.

The main characteristic features of the entangled molecular initial states in our H-H model, as compared to the unentangled atomic direct-product ones, are as follows: (i) the immediate response of atom B to the laser excitation of atom A, and (ii) the existence of fast out-of-phase oscillations of the ‘atomic’ energies  $E_A(t)$  and  $E_B(t)$  after the end of the applied laser pulse. These features should occur in a long-range quantum communication among distant quantum systems for the follow-

ing reason. The time-dependent ‘atomic’ energies  $E_A(t)$  and  $E_B(t)$  represent the information encoded in the laser pulse. Therefore, if only one atom A of the entangled A-B pair is excited by the laser pulse, the encoded information reaches atom B (receiver) instantaneously and, moreover, can be decoded both during and after the end of the pulse acting on atom A.

We have found that in the case of a narrow spatial envelope of an applied laser pulse, which excites only electrons belonging to atom A, the ‘sequential’ EER-induced ionization of atom B is more efficient than the laser-induced ionization of atom A [see Figs. 2(f) and 6(e)]. These results suggest important consequences for more complex quantum systems, e.g. those composed of three and more distant sub-systems, such as  $\{A_n\}$ ,  $n = 1, 2, \dots, N$ . If we excite by a laser pulse with a narrow spatial envelope only sub-system  $A_1$ , for example, and if ionization probabilities obey  $I_{A_n} < I_{A_{n+1}}$ , we can stimulate an efficient chain of ‘sequential’ ionization events with ever increasing probability in the total  $\{A_n\}$  system. The same may also apply to the energy transfer in the  $\{A_n\}$  system. To achieve such collective energy transfer and ‘sequential’ ionization, a narrow spa-

tial shaping of the laser field as reported in [7] needs further exploration. To achieve the condition  $I_{A_n} < I_{A_{n+1}}$  in the  $\{A_n\}$  systems with a Gaussian spatial envelope of Eq.(14), we can always choose  $z_0 < 0$  such that the effective-field amplitudes obey  $\mathcal{E}_0^{A_n} > \mathcal{E}_0^{A_{n+1}}$ . In this case we can anticipate that the condition  $I_{A_n} < I_{A_{n+1}}$  is fulfilled at the edge of the Gaussian envelope.

Finally, at a shorter pulse duration and/or at a smaller laser carrier frequency, such that the number of optical cycles per pulse is  $N_c < 15$  (see Ref. [9]), the role of CEP-effects as explored previously in LIET [11] offers new avenues for energy and information transfer at long-range distances.

## ACKNOWLEDGMENTS

This work has been financially supported by the Deutsche Forschungsgemeinschaft through the Sfb 652 (G.K.P., O.K.) which is gratefully acknowledged, and A.D.B. thanks the Humboldt Foundation for the financial support through a Humboldt Research Award.

- 
- [1] L.S. Cederbaum, J.Zobeley, and F. Tarantelli, Phys. Rev. Lett. **79**, 4778 (1997).
  - [2] S. Marburger, O. Kugeler, U. Hergenhahn, T. Möller, Phys. Rev. Lett. **90**, 203401 (2003).
  - [3] T. Jahnke, A. Czasch, M.S. Schöffler, S. Schössler, A. Knapp, M. Kasz, J. Titze, C. Wimmer, K. Kreidi, R.E. Grisenti, A. Staudte, O. Jagutzki, U. Hergenhahn, H. Schmidt-Böcking, R. Dörner, Phys. Rev. Lett. **93**, 163401 (2004).
  - [4] Y. Morishita, X.-J. Liu, N. Saito, T. Lischke, M. Kato, G. Prumper, M. Oura, H. Yamaoka, Y. Tamenori, I.H. Suzuki, K. Ueda, Phys. Rev. Lett. **96**, 243402 (2006).
  - [5] P. Lablanquie, T. Aoto, Y. Hikosaka, Y. Morioka, F. Penent, K. Ito, J. Chem. Phys. **127**, 154323 (2007).
  - [6] T. Jahnke, H. Sann, T. Havermeier, K. Kreidi, C. Stuck, M. Meckel, M. Schöffler, N. Neumann, R. Wallauer, S. Voss, A. Czasch, O. Jagutzki, A. Malakzadeh, F. Afaneh, T. Weber, H. Schmidt-Böcking, R. Dörner, Nature Phys. **6**, 74 (2010).
  - [7] T. Havermeier, T. Jahnke, K. Kreidi, R. Wallauer, S. Voss, M. Schöffler, S. Schössler, L. Foucar, N. Neumann, J. Titze, H. Sann, M. Kuhn, J. Voigtsberger, J.H. Morrilla, W. Schollkopf, H. Schmidt-Böcking, R.E. Grisenti, R. Dörner, Phys. Rev. Lett. **104**, 133401 (2010).
  - [8] N. Sisourat, N.V. Kryzhevoi, P. Kolorenč, S. Scheit, T. Jahnke, L.S. Cederbaum, Nature Phys. **6**, 508 (2010).
  - [9] S. Chelkowski and A.D. Bandrauk, Phys. Rev. A **65**, 061802 (2002).
  - [10] A.D. Bandrauk, S. Chelkowski, S. Kawai, and H. Lu, Phys. Rev. Lett. **101**, 153901 (2008).
  - [11] A.D. Bandrauk, S.Barmaki, and G.L. Kamta, Phys. Rev. Lett. **98**, 013001 (2007).
  - [12] V. May, O. Kühn, *Charge and Energy Transfer Dynamics in Molecular System*, 2nd revised and enlarged edition, (Wiley-VCH, Weinheim, 2004); A. Nitzan, *Chemical Dynamics in Condensed Phases*, (Oxford, University Press, 2006).
  - [13] A.D. Bandrauk and N.H. Shon, Phys. Rev. A **66**, 013401(R) (2002); Phys. Rev. A **81**, 062101 (2010).
  - [14] N. Došlić, Phys. Rev. A **74**, 013402 (2006).
  - [15] G.K. Paramonov, Chem. Phys. Lett. **411**, 350 (2005); Chem. Phys. **338**, 329 (2007).
  - [16] M. Kaluža, J.T. Muckerman, P. Gross, and H. Rabitz, J. Chem. Phys. **100**, 4211 (1994).
  - [17] M.V. Fedorov, M.A. Efremov, A.E. Kazakov, K.W. Chan, C.K. Law, and J.H. Eberly, Phys. Rev. A **69**, 052117 (2004).
  - [18] D. Petrosyan, G. Kurizki, and M. Shapiro, Phys. Rev. A **67**, 012318 (2003).
  - [19] G. Burkard, D. Loss, and D.P. DiVincenzo, Phys. Rev. B **59**, 2070 (1999).
  - [20] T. Wilk, A. Gaëtan, C. Evellin, J. Wolters, Y. Miroshnychenko, P. Grangier, and A. Browaeys, Phys. Rev. Lett. **104**, 010502 (2010).
  - [21] A. Ishizaki and G.R. Fleming, New J. Phys. **12**, 055004 (2010).
  - [22] H. Kono, Y. Sato, N. Tanaka, T. Kato, K. Nakai, S. Koseki, and Y. Fujimura, Chem. Phys. **304**, 203 (2004).
  - [23] P.B. Corkum, Phys. Rev. Lett. **71**, 1994 (1993).
  - [24] K.-J. Yuan and A.D. Bandrauk, Phys. Rev. A **80**, 053404 (2009).